RSC Advances

PAPER

View Article Online
View Journal | View Issue

Cite this: *RSC Adv.*, 2022, **12**, 8283

One-step solvent-free synthesis of carbon dot-based layered composites exhibiting color-tunable photoluminescence†

Junya Uchida, ‡* Yuka Takahashi, Takumi Katsurao and Hiroshi Sakabe

Received 16th January 2022
Accepted 10th March 2022

DOI: 10.1039/d2ra00312k

rsc.li/rsc-advances

We here report a practical and green approach to the development of luminescent composites through *in situ* solvent-free formation of carbon dots on layered inorganic compounds. The composites exhibit higher solid-state photoluminescence than those prepared by mixing of synthesized carbon dots and layered clay minerals. Tuning of the emission color of the composites has also been achieved by the addition of small molecules into phloroglucinol as starting materials for carbonization. The carbon dots synthesized in clay compounds in the solvent-free conditions are well-dispersed to obtain homogeneous composites. Furthermore, we have demonstrated that highly luminescent carbon dots are formed by carbonization in the presence of layered inorganic compounds. The one-step solvent-free approach presented in this work may allow not only facile, economical, and sustainable production of nanostructured carbon dot-based composites but also improvement of their luminescence properties.

Introduction

Carbon dots (CDs) have attracted much attention as a new class of carbon-based functional nanomaterials.[1–6] In particular, metal-free luminescent CDs are less toxic and have the potential to exhibit optical properties comparable to conventional semiconductor quantum dots.[7–12] Recently, green synthesis of these CDs has been intensively explored for the industrial production of CD-based materials towards a future sustainable society.[13–18]

Our intention here is to demonstrate practical solvent-free synthesis of CDs in layered inorganic compounds as a green process to form luminescent composites (Fig. 1). Layered inorganic compounds are anisotropic host materials that can incorporate organic molecules and metal ions inside their interlayer spaces.[19–32] A variety of chemical reactions utilizing the surface and nanospace of layered compounds have also been studied.[33–39] Among these layered compounds, clay minerals have been widely used as components for the development of functional materials because they are abundant, low-cost, biocompatible, and environmentally friendly.[19–21,33–38,40–48]

CD-based composites with enhanced stability and functions have been prepared by combining CDs with inorganic materials.[49–60] Although the combination of layered clay minerals and CDs was reported,[57–60] little is known about one-step solvent-free approach to the synthesis of luminescent CD-based composites. We envisaged that this approach would lead to facile, economical, and green production of CD-based nanostructured composites as well as improvement of thermal and photoluminescence properties.

Herein, we report on one-step solvent-free synthesis of CD-based luminescent layered composites (Fig. 1). The *in situ* preparation of CDs on layered inorganic compounds was expected to allow the dispersion and controlled synthesis of CDs

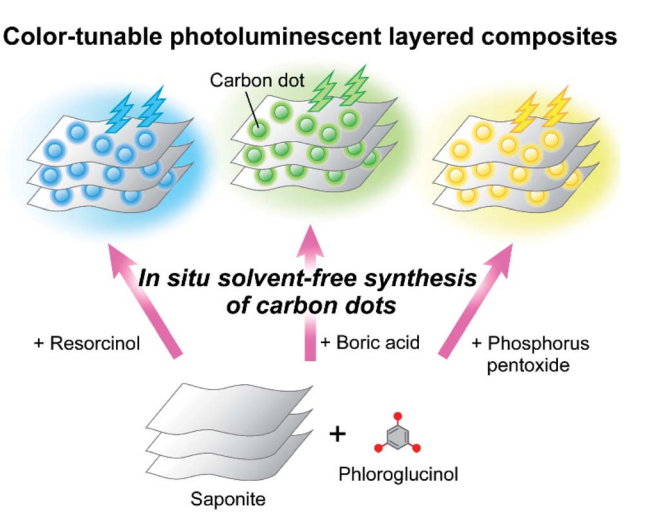

Fig. 1 Schematic illustration of one-step solvent-free synthesis of carbon dot-based color-tunable photoluminescent layered composites.

Advanced Research Department, Kureha Corporation, Ochiai, Nishiki-Machi, Iwaki, Fukushima 974-8686, Japan

† Electronic supplementary information (ESI) available. See DOI: 10.1039/d2ra00312k

‡ Present address: Department of Chemistry and Biotechnology, School of Engineering, The University of Tokyo, Hongo, Bunkyo-ku, Tokyo 113-8656, Japan. E-mail: j_uchida@chembio.t.u-tokyo.ac.jp.

to achieve efficient luminescence of the composites in the solid states. Tuning of the luminescence color was also intended by addition of low-molecular-weight compounds into phloroglucinol as starting materials for carbonization. Furthermore, the structures of CDs formed in the layered compounds were examined to understand luminescence properties of the composites.

Results and discussion

Material design

Phloroglucinol was selected as a carbon source for the formation of emissive CDs.[10] Carbonization of phloroglucinol on saponite under solvent-free conditions was expected to directly provide solid-state luminescent CD-based composites with thermal stability (**P-CD1**/saponite). Combination of carbon sources and doping of heteroatoms for the preparation of carbon-based nanomaterials have been shown to control their functions.[1–6,61–64] Thus, addition of resorcinol, boric acid, and phosphorus pentoxide to phloroglucinol followed by thermal treatment in the presence of saponite would lead to tuning of the emission color of the CD-based composites (**PR-CD1**/saponite, **PB-CD1**/saponite, and **PP-CD1**/saponite, respectively) (Fig. 1). The composites obtained by the *in situ* formation of CDs were considered to exhibit efficient luminescence because of homogeneous dispersion of CDs in the composites. We also envisioned that the carbonization in layered inorganic compounds may control the formation of π-conjugated structures of CDs.[34] For comparison, the **P-CD2**/saponite, **PR-CD2**/saponite, **PB-CD2**/saponite, and **PP-CD2**/saponite composites obtained by mixing of synthesized CDs and saponite were designed to study the luminescence properties.

Thermal properties of the carbon dots and their composites

The CD-based layered composites exhibited better thermal stability than CDs without clay minerals (Fig. 2 and S1†). Fig. 2 shows thermogravimetric (TG) curves of the **P-CD1**(10)/saponite, **P-CD1**(21)/saponite, and **P-CD1**(40)/saponite composites containing 10, 21, 40 wt% of CDs, respectively. After dehydration of adsorbed water around 150 °C, weight losses of the decomposition of CDs were observed from 300 °C to 500 °C for the **P-CD1**/saponite composites. Another weight loss around 700 °C was characteristic of dehydroxylation of the clay minerals.[65] For **P-CD1**, which was extracted from the **P-CD1**(21)/saponite composite, the TG curve showed a gradual weight loss from 100 °C (Fig. 2). The decomposition temperature of **P-CD1** was much lower than those of CDs in the **P-CD1**/saponite composites. Hybridization of CDs with clay minerals led to the improvement of thermal stability of the composites.

Hybrid structures of the composites

The nanostructures of the CD-based composites were examined by X-ray diffraction (XRD) measurements (Fig. 3). The basal spacing of saponite treated at 200 °C under N_2 flow for 3 h was about 10.5 Å (Fig. 3, top), whereas the spacing of the **P-CD1**(21)/saponite composite increased up to about 14.6 Å by the formation of CDs (Fig. 3, bottom). In addition, the layered structure of the **P-CD1**(21)/saponite composite was slightly disordered as compared to that of saponite because the peak at 14.6 Å was broader. These results suggest that the CDs were formed in the interlayer space of saponite.[33–35,37,39] As a comparison with the **P-CD1**(21)/saponite composite, the structure of the **P-CD2**(21)/saponite composite, which was prepared by mixing of **P-CD2** and saponite, was also studied. XRD pattern of the **P-CD2**(21)/saponite composite exhibited several sharp diffraction peaks (see ESI, Fig. S2†). These peaks can be attributed to the aggregation of **P-CD2** (see ESI, Fig. S2†). CDs have tendency to form aggregates because of their strong intermolecular interactions,[1,2,4,6] and therefore macroscopic phase separation was observed for the **P-CD2**(21)/saponite composite.

Scanning electron microscope (SEM) images of the composites were obtained to study the hybrid structures (Fig. 4 and S3†). Fig. 4a shows that the **P-CD1**(21)/saponite composite possessed wave-like nanostructures. Similar morphologies were also observed for pristine saponite (see ESI, Fig. S4†), indicating

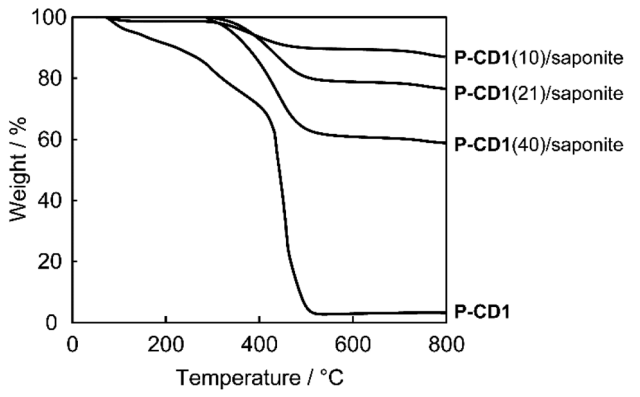

Fig. 2 TG curves of P-CD1 and the P-CD1/saponite composites with different ratios of CDs.

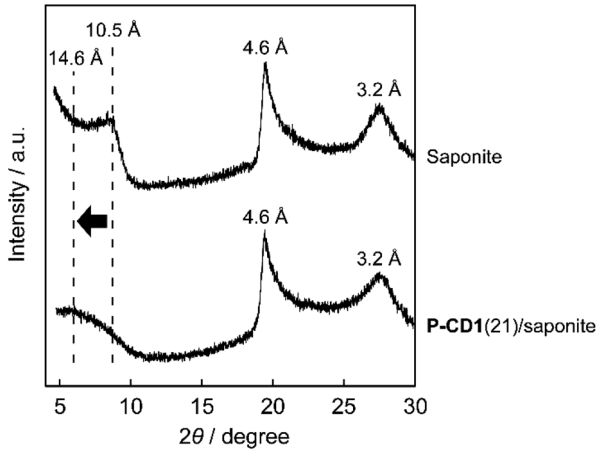

Fig. 3 XRD patterns of saponite and the P-CD1(21)/saponite composite.

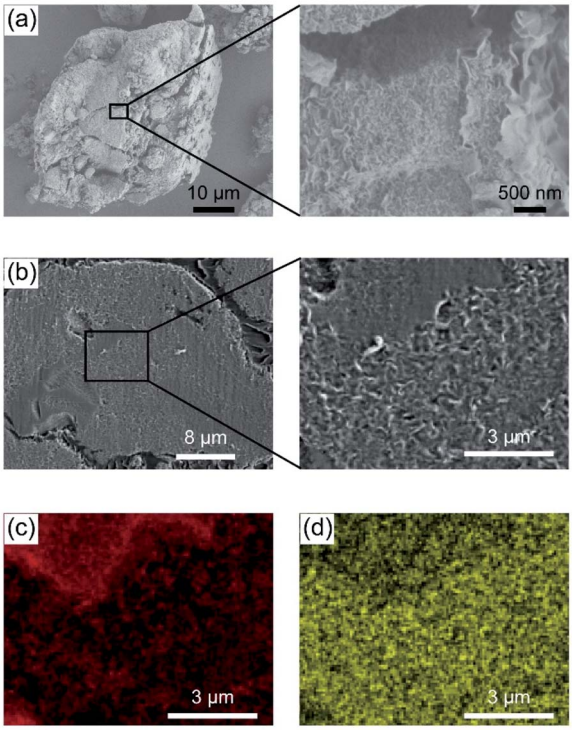

Fig. 4 (a) SEM images of the P-CD1(21)/saponite composite. Comparison of (b) SEM images with (c) C and (d) Si mapping of the cross section of the P-CD1(21)/saponite composite.

that the layered assembly of saponite was preserved after the formation of CDs. The cross-sectional SEM images of a particle of the **P-CD1**(21)/saponite composite are shown in Fig. 4b. The cross section was analyzed by energy dispersive X-ray (EDX) spectrometer to characterize the distribution of CDs inside the particles of the composites (Fig. 4c and d). The mapping images of C Kα and Si Kα X-ray suggest that CDs were dispersed inside the **P-CD1**(21)/saponite composite. For the **P-CD2**(21)/saponite composite, SEM and EDX analysis revealed the deposition of aggregates of CDs on saponite (see ESI, Fig. S5†). These observations were consistent with the results of XRD measurements of the **P-CD2**(21)/saponite composites.

The effects of the ratios of CDs on specific surface area of the **P-CD1**/saponite and **P-CD2**/saponite composites were investigated. Fig. 5 shows Brunauer–Emmett–Teller (BET) specific surface area of these composites with different ratios of CDs. The specific surface area of the **P-CD1**/saponite composites remarkably decreased with an increasing weight percentage of CDs (Fig. 5, solid line). This observation suggests that the CDs were incorporated into the porous structure of saponite to decrease the surface area of the composites. It should be noted that specific surface area of the **P-CD1**(21)/saponite composite was over 100 times lower than that of the **P-CD2**(21)/saponite composite, even though the ratio of CDs in each composite was almost the same. These results indicate that CDs synthesized *in situ* were efficiently embedded in the pores including the interlayer space of saponite, which prevented aggregation of CDs in the composites.

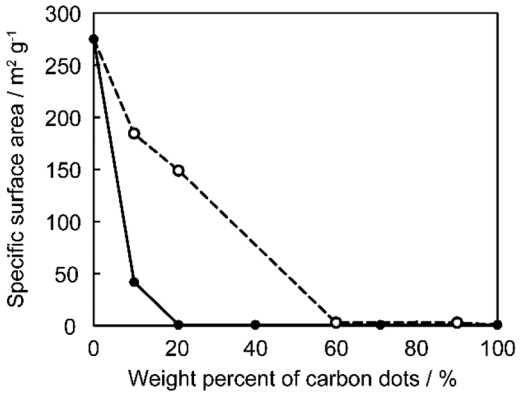

Fig. 5 Specific surface area of the P-CD1/saponite (solid line) and P-CD2/saponite composites (dashed line).

Luminescence properties of the composites

The composites obtained by the *in situ* synthesis exhibited luminescence in the solid states under the illumination of UV light (Fig. 6a–d). For example, the **P-CD1**(10)/saponite composite showed blue-green emission (Fig. 6a). It is noteworthy that tuning of the luminescence color was achieved by the introduction of additives into the starting materials for the synthesis of CD-based composites. The **PR-CD1**/saponite composite prepared by using phloroglucinol and resorcinol exhibited blue luminescence (Fig. 6b), whereas the **PB-CD1**/saponite composite prepared by using phloroglucinol and boric acid displayed yellow-green luminescence (Fig. 6c). The yellow-

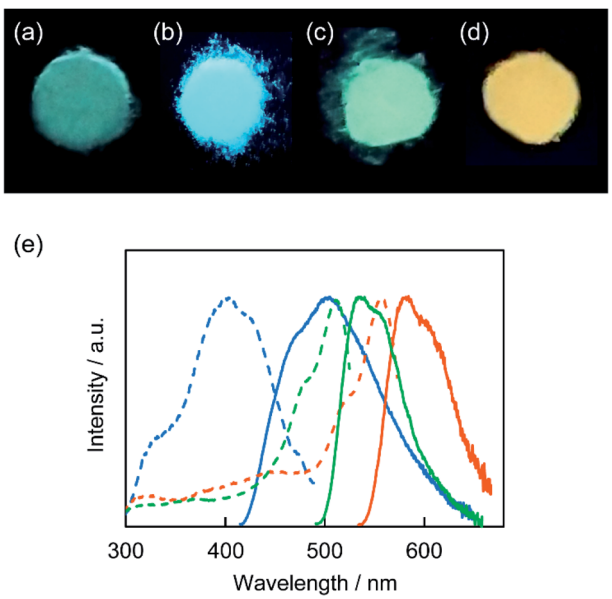

Fig. 6 Photographs of (a) P-CD1(10)/saponite, (b) PR-CD1/saponite, (c) PB-CD1/saponite, and (d) PP-CD1/saponite composites in the solid states under UV light irradiation (λ_{ex} = 365 nm). (e) Normalized excitation (dashed lines) and emission spectra (solid lines) of the PR-CD1/saponite (indicated in blue, λ_{em} = 500 nm, λ_{ex} = 400 nm), PB-CD1/saponite (green, λ_{em} = 535 nm, λ_{ex} = 480 nm), and PP-CD1/saponite composites (orange, λ_{em} = 585 nm, λ_{ex} = 520 nm) in the solid states.

orange emission was observed for the **PP-CD1**/saponite composite prepared by using phloroglucinol and phosphorus pentoxide (Fig. 6d).

The excitation and emission spectra of the **PR-CD1**/saponite, **PB-CD1**/saponite, and **PP-CD1**/saponite composites in the solid states were obtained to study the photophysical properties (Fig. 6e). The **PR-CD1**/saponite composite exhibited an emission band centered at 500 nm, which was blue-shifted from that for the **P-CD1**(10)/saponite composite (525 nm, see ESI, Fig. S6†). This difference was likely due to the formation of CDs containing smaller π-conjugated structures by the combination of resorcinol and phloroglucinol as carbon sources.[10] The **PB-CD1**/saponite composite exhibited a slightly red-shifted emission at 535 nm as compared to the **P-CD1**(10)/saponite composite. Further bathochromic shift was observed in the emission for the **PP-CD1**/saponite composite probably due to the introduction of phosphorus into the CDs through carbonization.[66–68] On the other hand, the UV-vis spectra of **PB-CD1**/saponite and **PP-CD1**/saponite composites showed small absorption peaks at 507 and 550 nm, respectively (see ESI, Fig. S7†). The wavelengths of these peaks corresponded to those of the peaks in the excitation spectra (Fig. 6e).

The photoluminescence quantum yields (Φ_{PL}) of the composites were measured. The **P-CD1**(10)/saponite, **P-CD1**(21)/saponite, **PR-CD1**/saponite, **PB-CD1**/saponite, and **PP-CD1**/saponite composites exhibited the photoluminescence efficiency of 0.04, 0.05, 0.07, 0.29, and 0.15 in the solid states, respectively. The enhanced emission of the **PB-CD1**/saponite and **PP-CD1**/saponite composites was probably attributed to the fixation of molecular motion through the interactions between the CDs and saponite. In contrast, the **P-CD2**(10)/saponite, **P-CD2**(21)/saponite, **PR-CD2**/saponite, **PB-CD2**/saponite, and **PP-CD2**/saponite composites, which were prepared by mixing of synthesized CDs and saponite, showed no significant emission by visual inspection under UV light irradiation. The Φ_{PL} values of these composites were less than 0.01. The higher Φ_{PL} values of the composites prepared by the *in situ* synthesis of CDs on saponite were partly due to the suppression of aggregation-caused quenching through the dispersion of fluorescent CDs in the composites.

Structure and luminescence properties of the carbon dots

The structures of the CDs were examined to provide further insight into the higher luminescence efficiency of the composites prepared by the one-step solvent-free method. For this purpose, the X-ray photoelectron spectroscopy (XPS) of **P-CD1** and **P-CD2** was carried out to study the chemical state of elements. Notably, the high-resolution XPS analysis of C 1s peaks showed that a peak ascribed to C–C bonds was more distinct for **P-CD1** (Fig. 7). The percentage of C–C peaks in **P-CD1** and **P-CD2** was estimated to be 48% and 37%, respectively (see ESI, Fig. S8†). The C/O ratio of **P-CD1** and **P-CD2** was almost the same (2.3 and 2.2, respectively), while that of phloroglucinol was 1.5. These results indicate that condensation of phloroglucinol for the formation of **P-CD1** was affected by saponite to give more C–C bonds in the chemical structures. It was

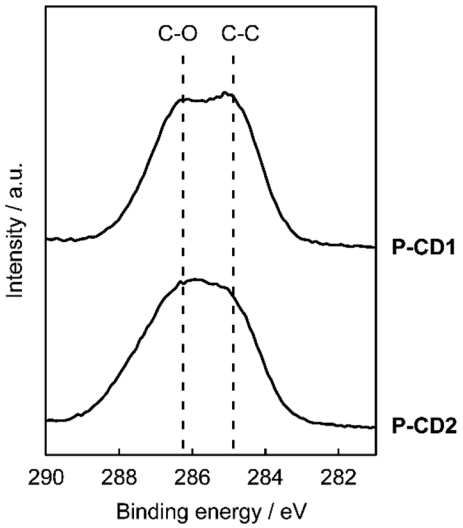

Fig. 7 C 1s XPS analysis of P-CD1 and P-CD2.

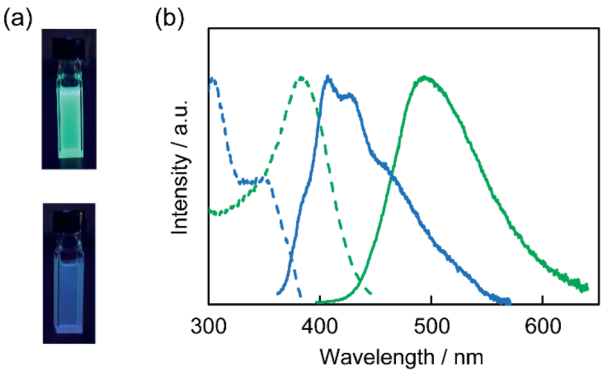

Fig. 8 (a) Photographs of P-CD1 (top) and P-CD2 (bottom) in methanol solution (1 g L^{-1}) under UV light irradiation (λ_{ex} = 365 nm). (b) Normalized excitation (dashed lines) and emission spectra (solid lines) of P-CD1 (indicated in green, λ_{em} = 495 nm, λ_{ex} = 380 nm) and P-CD2 (blue, λ_{em} = 410 nm, λ_{ex} = 340 nm) in methanol solution (1 g L^{-1}).

previously reported that carbonization of polyacrylonitrile in the two-dimensional space between montmorillonite lamellae produced graphite-like structures more efficiently.[34] The carbonization of phloroglucinol confined in the interlayer space of saponite may result in the formation of larger π-conjugated structures with more C–C bonds for **P-CD1**.[10]

Emission properties of **P-CD1** and **P-CD2** in solution were explored. The methanol solution of **P-CD1** displayed green emission (Fig. 8a, top), while that of **P-CD2** exhibited blue emission (Fig. 8a, bottom). The wavelengths of the excitation and emission maxima of **P-CD1** were red-shifted by 79 and 87 nm relative to those of **P-CD2**, respectively (Fig. 8b). The absorption of visible light for **P-CD1** was also stronger than that for **P-CD2** (see ESI, Fig. S9†). These results support the formation of extended π-conjugated structures for **P-CD1** as proposed by XPS analysis. The Φ_{PL} value of the methanol solution of **P-CD1** was 0.20, which was much higher than that of **P-CD2** (0.07). For **P-CD1** and **P-CD2** in the solid states, no emission was

observed under UV light irradiation. Overall, the efficient luminescence properties of the composites prepared by the one-step solvent-free approach can be attributed to the preferential formation of π-conjugated structures of CDs as well as dispersion of CDs in the composites.

Conclusions

In conclusion, we have demonstrated practical one-step solvent-free synthesis of CD-based luminescent layered composites by thermal treatment of the mixtures of carbon sources and saponite. The emission color of the composites was tuned by addition of small molecules into phloroglucinol as starting materials for carbonization. SEM observation revealed that CDs synthesized *in situ* were well-dispersed in saponite, which led to the solid-state emission and high thermal stability of the composites. Moreover, the solvent-free *in situ* synthesis of CDs on saponite allowed the formation of CDs with enhanced emission efficiency. The facile and green preparation of nanostructured CD-based composites would have potential towards sustainable development of new optical functional materials.

Experimental section

Materials

A synthetic saponite (Sumecton SA) was purchased from Kunimine Industries. Other reagents were purchased from Tokyo Kasei, Aldrich, FUJIFILM Wako Pure Chemical, and used as received without further purification.

Preparation of composites of carbon dots and saponite

P-CD1/saponite composites. A ground mixture of 0.15 g phloroglucinol dihydrate and 1.0 g saponite was heated at 200 °C under N_2 flow for 3 h to give **P-CD1**/saponite containing around 10 wt% of CDs (**P-CD1**(10)/saponite). **P-CD1**(21)/saponite, **P-CD1**(40)/saponite, and **P-CD1**(71)/saponite were prepared in a similar manner except that a ground mixture of 0.4 g phloroglucinol dihydrate and 1.0 g saponite, 1.0 g phloroglucinol dihydrate and 1.0 g saponite, and 0.8 g phloroglucinol dihydrate and 0.2 g saponite were used, respectively. The ratios of CDs in the composites were estimated by TG measurements.

PR-CD1/saponite composites. A ground mixture of 0.02 g phloroglucinol dihydrate, 0.1 g resorcinol, and 1.0 g saponite was heated at 200 °C under N_2 flow for 3 h to give **PR-CD1**/saponite.

PB-CD1/saponite composites. A ground mixture of 0.15 g phloroglucinol dihydrate, 0.057 g boric acid, and 1.0 g saponite was heated at 200 °C under N_2 flow for 3 h to give **PB-CD1**/saponite.

PP-CD1/saponite composites. A ground mixture of 0.15 g phloroglucinol dihydrate, 0.13 g phosphorus pentoxide, and 1.0 g saponite was heated at 200 °C under N_2 flow for 3 h to give **PP-CD1**/saponite.

P-CD2/saponite composites. Phloroglucinol dihydrate was heated at 200 °C under N_2 flow for 3 h to form **P-CD2**. The **P-CD2**(10)/saponite composite was obtained by grinding 0.1 g **P-CD2** with 0.9 g saponite. The **P-CD2**(21)/saponite, **P-CD2**(60)/saponite, and **P-CD2**(90)/saponite composites were also prepared by grinding 0.21 g **P-CD2** with 0.79 g saponite, 0.6 g **P-CD2** with 0.4 g saponite, and 0.9 g **P-CD2** with 0.1 g saponite, respectively.

PR-CD2/saponite composites. A ground mixture of 0.02 g phloroglucinol dihydrate and 0.1 g resorcinol was heated at 200 °C under N_2 flow for 3 h to form **PR-CD2**. The **PR-CD2**/saponite composite was obtained by grinding 0.05 g **PR-CD2** with 0.45 g saponite.

PB-CD2/saponite composites. A ground mixture of 0.15 g phloroglucinol dihydrate and 0.057 g boric acid was heated at 200 °C under N_2 flow for 3 h to form **PB-CD2**. The **PB-CD2**/saponite composite was obtained by grinding 0.1 g **PB-CD2** with 0.9 g saponite.

PP-CD2/saponite composites. A ground mixture of 0.15 g phloroglucinol dihydrate and 0.13 g phosphorus pentoxide was heated at 200 °C under N_2 flow for 3 h to form **PP-CD2**. The **PP-CD2**/saponite composite was obtained by grinding 0.1 g **PP-CD2** with 0.9 g saponite.

Extraction of carbon dots from the carbon dot/saponite composites

Carbon dot **P-CD1** was obtained by extraction from the **P-CD1**(21)/saponite composite with methanol. After removing precipitates by centrifugation, the methanol solution was dried under vacuum to give **P-CD1** as a brown solid.

Characterization

Thermogravimetric (TG) measurements were performed with Mettler TGA 2 up to 800 °C at a heating rate of 10 °C min^{-1} under air flow (40 mL min^{-1}). Powder X-ray diffraction (XRD) measurements were carried out with PANalytical X'PERT-PRO MPD using Ni-filtered Cu Kα radiation. The morphologies of the composites were observed with a Hitachi SU8220 field-emission scanning electron microscope (SEM) operated at 1 kV. Energy dispersive X-ray (EDX) analysis was performed using a Bruker XFlash 5060FQ energy dispersive X-ray spectroscope. Brunauer–Emmett–Teller (BET) specific surface area was measured using Quantachrome Monosorb. The adsorbed gas was N_2 (20%) and He (80%) at 77 K. Prior to the BET surface area measurements, the samples were dried under the gas flow at 150 °C for 10 min. UV-vis absorption measurements were conducted with Hitachi U-4100 and U-3900H spectrophotometers. Excitation and emission spectra and absolute photoluminescence quantum yields (Φ_{PL}) were obtained with JASCO FP-8500 spectrofluorometer equipped with an integrating sphere unit ILF-835. X-ray photoelectron spectroscopy (XPS) was carried out using JEOL JPS-9010MC.

Author contributions

J. U. conceived and designed the project with the help of T. K. and H. S. J. U. and Y. T. performed synthesis and characterization of materials. J. U. wrote the manuscript. All authors read and commented on the manuscript.

Conflicts of interest

There are no conflicts to declare.

Acknowledgements

We acknowledge Mr Shigeaki Miyazaki for SEM observations and Dr Kei Yanagisawa and Dr Takahiro Kudo for XPS measurements. We thank Dr Naoto Haneishi, Dr Ryoto Kojima, and Dr Masaki Ishizu for helpful discussions.

Notes and references

1 S. N. Baker and G. A. Baker, *Angew. Chem., Int. Ed.*, 2010, **49**, 6726.
2 S. Y. Lim, W. Shen and Z. Gao, *Chem. Soc. Rev.*, 2015, **44**, 362.
3 S. Zhu, Y. Song, X. Zhao, J. Shao, J. Zhang and B. Yang, *Nano Res.*, 2015, **8**, 355.
4 L. Xiao and H. Sun, *Nanoscale Horiz.*, 2018, **3**, 565.
5 X. T. Zheng, A. Ananthanarayanan, K. Q. Luo and P. Chen, *Small*, 2015, **11**, 1620.
6 F. Arcudi, L. Đorđević and M. Prato, *Acc. Chem. Res.*, 2019, **52**, 2070.
7 H. Sun, L. Wu, W. Wei and X. Qu, *Mater. Today*, 2013, **16**, 433.
8 X. Li, M. Rui, J. Song, Z. Shen and H. Zeng, *Adv. Funct. Mater.*, 2015, **25**, 4929.
9 M. Han, S. Zhu, S. Lu, Y. Song, T. Feng, S. Tao, J. Liu and B. Yang, *Nano Today*, 2018, **19**, 201.
10 F. Yuan, T. Yuan, L. Sui, Z. Wang, Z. Xi, Y. Li, X. Li, L. Fan, Z. A. Tan, A. Chen, M. Jin and S. Yang, *Nat. Commun.*, 2018, **9**, 2249.
11 J. Zhang and S.-H. Yu, *Mater. Today*, 2016, **19**, 382.
12 H. Liu, Z. Li, Y. Sun, X. Geng, Y. Hu, H. Meng, J. Ge and L. Qu, *Sci. Rep.*, 2018, **8**, 1086.
13 M. L. Liu, B. B. Chen, C. M. Li and C. Z. Huang, *Green Chem.*, 2019, **21**, 449.
14 V. Sharma, P. Tiwari and S. M. Mobin, *J. Mater. Chem. B*, 2017, **5**, 8904.
15 S. Chahal, J.-R. Macairan, N. Yousefi, N. Tufenkji and R. Naccache, *RSC Adv.*, 2021, **11**, 25354.
16 S. R. Ankireddy, V. G. Vo, S. S. A. An and J. Kim, *ACS Appl. Bio Mater.*, 2020, **3**, 4873.
17 K. Ravishankar, K. M. Shelly, A. Narayanan and R. Dhamodharan, *ACS Sustainable Chem. Eng.*, 2019, **7**, 13206.
18 S. Iravani and R. S. Varma, *Environ. Chem. Lett.*, 2020, **18**, 703.
19 E. Ruiz-Hitzky, *Adv. Mater.*, 1993, **5**, 334.
20 M. Ogawa and K. Kuroda, *Chem. Rev.*, 1995, **95**, 399.
21 T. E. Mallouk and J. A. Gavin, *Acc. Chem. Res.*, 1998, **31**, 209.
22 A. H. Khan, S. Ghosh, B. Pradhan, A. Dalui, L. K. Shrestha, S. Acharya and K. Ariga, *Bull. Chem. Soc. Jpn.*, 2017, **90**, 627.
23 M. Naguib, M. W. Barsoum and Y. Gogotsi, *Adv. Mater.*, 2021, **33**, 2103393.
24 K. Kawashima, M. Hojamberdiev, H. Wagata, K. Yubuta, K. Domen and K. Teshima, *ACS Sustainable Chem. Eng.*, 2017, **5**, 232.
25 Y. Oaki, H. Ohno and T. Kato, *Nanoscale*, 2010, **2**, 2362.
26 Y. Oaki, *Bull. Chem. Soc. Jpn.*, 2017, **90**, 776.
27 T. Nakato, K. Kuroda and C. Kato, *Chem. Mater.*, 1992, **4**, 128.
28 N. Miyamoto, K. Kuroda and M. Ogawa, *J. Am. Chem. Soc.*, 2001, **123**, 6949.
29 C. N. R. Rao, H. S. S. R. Matte and U. Maitra, *Angew. Chem., Int. Ed.*, 2013, **52**, 13162.
30 M. Tipplook, T. Sudare, H. Shiiba, A. Seki and K. Teshima, *ACS Appl. Mater. Interfaces*, 2021, **13**, 51186.
31 T. Sudare, S. Tamura, H. Tanaka, F. Hayashi and K. Teshima, *Inorg. Chem.*, 2019, **58**, 15710.
32 W. A. Haider, M. Tahir, L. He, H. A. Mirza, R. Zhu, Y. Han and L. Mai, *ACS Cent. Sci.*, 2020, **6**, 1901.
33 G. A. Ozin, *Adv. Mater.*, 1992, **4**, 612.
34 T. Kyotani, N. Sonobe and A. Tomita, *Nature*, 1988, **331**, 331.
35 K. Takagi, T. Shichi, H. Usami and Y. Sawaki, *J. Am. Chem. Soc.*, 1993, **115**, 4339.
36 A. Okada and A. Usuki, *Macromol. Mater. Eng.*, 2006, **291**, 1449.
37 R. Schöllhorn, *Chem. Mater.*, 1996, **8**, 1747.
38 Y. Ide, A. Fukuoka and M. Ogawa, *Chem. Mater.*, 2007, **19**, 964.
39 N. Yanai, T. Uemura, M. Ohba, Y. Kadowaki, M. Maesato, M. Takenaka, S. Nishitsuji, H. Hasegawa and S. Kitagawa, *Angew. Chem., Int. Ed.*, 2008, **47**, 9883.
40 E. Ruiz-Hitzky, M. Darder and P. Aranda, *J. Mater. Chem.*, 2005, **15**, 3650.
41 S. Takagi, T. Shimada, M. Eguchi, T. Yui, H. Yoshida, D. A. Tryk and H. Inoue, *Langmuir*, 2002, **18**, 2265.
42 Y. Zhou, A. M. LaChance, A. T. Smith, H. Cheng, Q. Liu and L. Sun, *Adv. Funct. Mater.*, 2019, **29**, 1807611.
43 V. Balakumar, K. Sekar, C. Chuaicham, R. Manivannan and K. Sasaki, *Environ. Sci.: Nano*, 2021, **8**, 2261.
44 T. Fujimura, T. Shimada, R. Sasai and S. Takagi, *Langmuir*, 2018, **34**, 3572.
45 T. Nakato and N. Miyamoto, *Materials*, 2009, **2**, 1734.
46 L. Wu, J. Liu, Y. Liu, R. Huang, N. Tang, X. Wang and L. Hu, *RSC Adv.*, 2021, **11**, 33399.
47 K. Srinivasarao, S. M. Prabhu, W. Luo and K. Sasaki, *Appl. Clay Sci.*, 2018, **163**, 46.
48 P. Koilraj, Y. Kamura and K. Sasaki, *ACS Sustainable Chem. Eng.*, 2018, **6**, 13854.
49 J. Li, B. Wang, H. Zhang and J. Yu, *Small*, 2019, **15**, 1805504.
50 F. Wang, Z. Xie, H. Zhang, C. Liu and Y. Zhang, *Adv. Funct. Mater.*, 2011, **21**, 1027.
51 J. Zong, Y. Zhu, X. Yang, J. Shen and C. Li, *Chem. Commun.*, 2011, **47**, 764.
52 Z. Wang, C. Xu, Y. Lu, F. Wu, G. Ye, G. Wei, T. Sun and J. Chen, *ACS Appl. Mater. Interfaces*, 2017, **9**, 7392.
53 K. Hayashi, S. Ogawa, H. Watanabe, Y. Fujimaki, Y. Oaki and H. Imai, *Bull. Chem. Soc. Jpn.*, 2019, **92**, 1170.
54 A. B. Bourlinos, A. Stassinopoulos, D. Anglos, R. Zboril, V. Georgakilas and E. P. Giannelis, *Chem. Mater.*, 2008, **20**, 4539.
55 J. Liu, N. Wang, Y. Yu, Y. Yan, H. Zhang, J. Li and J. Yu, *Sci. Adv.*, 2017, **3**, e1603171.

56 M. Zhang, Q. Yao, C. Lu, Z. Li and W. Wang, *ACS Appl. Mater. Interfaces*, 2014, **6**, 20225.
57 Y. Zhai, F. Shen, X. Zhang, P. Jing, D. Li, X. Yang, D. Zhou, X. Xu and S. Qu, *J. Colloid Interface Sci.*, 2019, **554**, 344.
58 Y. Yu and L. Yan, *Bull. Chem. Soc. Jpn.*, 2017, **90**, 1217.
59 Y. Deng, P. Li, H. Jiang, X. Jia and H. Li, *J. Mater. Chem. C*, 2019, **7**, 13640.
60 J. Gogoi, S. Shishodia and D. Chowdhury, *RSC Adv.*, 2020, **10**, 37545.
61 Q. Xu, T. Kuang, Y. Liu, L. Cai, X. Peng, T. S. Sreeprasad, P. Zhao, Z. Yue and N. Li, *J. Mater. Chem. B*, 2016, **4**, 7204.
62 Y. Zhou and Y. Nishina, *Nanoscale Adv.*, 2020, **2**, 4417.
63 M. S. Ahmad and Y. Nishina, *Nanoscale*, 2020, **12**, 12210.
64 J. Tan, Y. Han, L. He, Y. Dong, X. Xu, D. Liu, H. Yan, Q. Yu, C. Huang and L. Mai, *J. Mater. Chem. A*, 2017, **5**, 23620.
65 N. Nityashree, U. K. Gautam and M. Rajamathi, *Appl. Clay Sci.*, 2014, **87**, 163.
66 M. K. Barman, B. Jana, S. Bhattacharyya and A. Patra, *J. Phys. Chem. C*, 2014, **118**, 20034.
67 K. S. Prasad, R. Pallela, D.-M. Kim and Y.-B. Shim, *Part. Part. Syst. Charact.*, 2013, **30**, 557.
68 G. Kalaiyarasan, J. Joseph and P. Kumar, *ACS Omega*, 2020, **5**, 22278.